**Membrane and Water Treatment**, *Vol. 11*, *No. 5 (2020) 353-361*
DOI: https://doi.org/10.12989/mwt.2020.11.5.353


# Numerical study of desalination by Sweeping Gas Membrane Distillation

Nizar Loussif*[1,2] and Jamel Orfi[3,4]

[1]*École Nationale d'Ingénieurs de Monastir, Université de Monastir, Monastir, Tunisie*
[2]*Département Génie des Procédés, Institut Supérieur des Etudes Technologiques Ksar Hellal, Tunisie*
[3]*Mechanical Engineering Department, King Saud University, Riyadh, KSA*
[4]*KA.CARE Energy Research and Innovation Center at Riyadh, Saudi Arabia*

*(Received April 30, 2020, Revised September 6, 2020, Accepted September 22, 2020)*

**Abstract.** The present study deals with a numerical investigation of heat and mass transfer in a Sweeping Gas Membrane Distillation (SGMD) used for desalination. The governing equations expressing the conservation of mass, momentum, energy and species with coupled boundary conditions were solved numerically. The slip boundary condition applied on the feed saline solution-hydrophobic membrane interface is taken into consideration showing its effects on profiles and process parameters.The numerical model was validated with available experimental data and was found to be in good agreement particularly when the slip condition is considered. The results of the simulations highlighted the effect of slip boundary condition on the velocity and temperature distributions as well as the process effectiveness. They showed in particular that as the slip length increases, the permeate flux of fresh water and process thermal efficiency rise.

**Keywords:** membrane distillation, desalination, heat and mass transfer, slip flow, SGMD

## 1. Introduction

Nowadays, many techniques are widely used to produce pure water from brackish or sea water. A promising technique, membrane distillation (MD) has many advantages particularly its low energy consumption, high quality water production and its ability to treat highly concentrated waters. In Membrane distillation, a hydrophobic membrane is used to ovoid membrane wetting and permitting only vapor transport to cross it. The driving force is the difference in vapor pressure of water caused by a temperature difference across the membrane. In fact, vapor molecules are transported from the high vapor pressure side to the low vapor pressure side. This vapor pressure difference may be maintained with one of the four following possibilities applied on the permeate side which leads to four different configurations (Rommel et al. 2007 and El-Bouraoui et al. 2016):

- Air Gap Membrane Distillation (AGMD): an air gap is placed between the membrane and a condensation surface; the water vapor molecules cross the membrane and the stagnant air and condense on the internal side of a cooling plate.
- Direct Contact Membrane Distillation (DCMD): an aqueous solution colder than the feed solution maintained in the direct contact with the permeate side.
- Vacuum Membrane Distillation (VMD): a vacuum pump can be used to reduce the pressure in the permeate side; the condensation occurs outside of the membrane module.
- Sweeping Gas Membrane Distillation (SGMD): a cold inert gas sweeps the permeate side carrying the water vapor molecules outside the membrane module where the condensation takes place.

Many theoretical and experimental studies have been conducted to investigate the MD performance, while SGMD configuration has received less attention. SGMD investigations have been conducted to show the process performance in particular pure water production and the thermal efficiency for isopropanol or ethanol water separation (Lee and Won 2001, Shukla *et al.* 2018), waste water containing ammonia (Xie et al. 2009), desalination (Khayet *et al.* 2003, Si *et al.* 2019, Moore *et al.* 2018), sucrose aqueous solutions (Cojocaru and Khayet 2011) and triethylene glycol (Duyen *et al.* 2016). In addition, theoretical studies concerned with the SGMD process have received less attention (Khayet *et al.* 2003, Loussif and Orfi 2016, Rivier *et al.* 2003 and Khayet *et al.* 2000) and few studies on SGMD have been done with advanced numerical analysis. The remaining studies are based on 1D simplified models using empirical heat and mass transfer correlations (El-Bouraoui *et al.* 2016, Lee and Won 2001, Xie *et al.* 2009, Camacho *et al.* 2013 and Charfi *et al*. 2010).

Furthermore, the non-slip boundary condition is always used at the hydrophobic side of the membrane, but when a surface is covered with hydrophobic material, the fluid near the surface does not stick to the solid boundary resulting in an overall velocity slip. This slip velocity is related to the normal velocity gradient of the fluid adjacent to the wall with a slip length *b* which can be described as the imaginary distance within the solid where the velocity extrapolates to

*Corresponding author, Professor
E-mail: loussif_nizare@yahoo.fr



ISSN: 2005-8624 (Print), 2092-7037 (Online)

zero. Slip velocity can be presented in the following form (Ramon *et al.* 2008):

$$U|_{y=0}=b\frac{\partial U}{\partial y}\Big|_{y=0} \quad (1)$$

Where $U$ is the axial velocity component [m/s], $b$ is the slip length [m] and y is the coordinate normal to the solution flow [m].

Pit *et al.* (2000) measured a slip length of 0.4 µm when the surface was coated with octadecyltrichlorosilane for hexadecane flowing between two rotating parallel disks. Cottin *et al.* (2005) investigated experimentally water flow across hydrophobic surfaces; they found slip lengths of approximately 0.02 µm. Tretheway and Meinhart (2002 and 2004) revealed an apparent fluid slip in channels with hydrophobic walls. They measured a slip length of about 1 µm. On the other hand, a superhydrophobic surface can dramatically reduce the hydrodynamic resistance and a slip length greater than 25 µm were measured by Ou and Rothstein (2005) and higher than 185 µm has been reported by Choi and Kim (2006) and Lee *et al.* (2008). Orfi *et al.* (2016) proposed a model for the heat and mass transfer in an air gap membrane distillation with slip flow. A recent work (Liu *et al.* (2020)) aimed to understand the reasons why superhydrophobic membrane is favorable for the MD technology in desalination use. Liu *et al.* (2020) developed models for the VMD establishing bridges between the membrane surface parameters and the heat and mass transfer mechanism. To the authors' knowledge, there is not study on the impact of slip flow conditions on the transport phenomena in SGMD.

Earlier studies on SGMD units used for desalination were performed within the continuum regime and the effect of slip flow at the hydrophobic membrane surface was neglected. Therefore, the aim of this study is to present a two-dimensional model for the transport phenomena in a SGMD configuration where the slip velocity boundary condition is considered. Parametric investigation will be undertaken to show the slip flow effects on profiles and process parameters.

## 2. Mathematical model

### 2.1 Process description

The configuration of a Sweeping Gas Membrane Distillation is a vertical channel one. It consists of two concentric channels. Hot saline water flows inside the inner one. The wall of the inner channel consists of a micro porous hydrophobic membrane through which only water vapor can diffuse and the liquid water is retained. The vapor is recovered through a sweeping gas to achieve the condensation outside the module. The feed water flows up while the air is forced to circulate in the opposite direction. Natural convection effects are ignored for both fluids saline water and air.

The computation domain includes the flows, heat and mass transfers in the hot saline water and the sweeping gas.

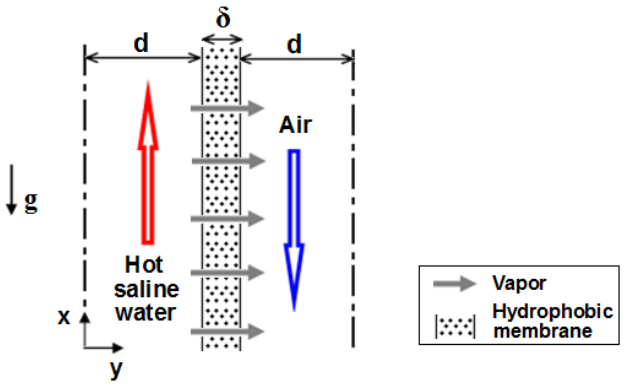


Fig. 1 Schematic diagram of a Sweeping Gas Membrane Distillation

The assumptions used in this study are: steady-state, axisymmetric and constant fluid properties. The flows are symmetric so that only half of the cells are shown and computed.

Fig. 1 describes the physical model considered in the present study.

### 2.2. Governing equations

In this section, we will present the governing equations and their boundary conditions for a SGMD process.

The partial differential equations governing the flow, heat and mass transfer within the hot feed saline solution and the sweeping air are those of conservation of mass, momentum energy and species in x and y directions. The suffixes $a$ and $s$ represent respectively the sweeping air and the hot saline solution.

These equations are normalized using the following dimensionless variables.

$$\bar{x}=\frac{x}{d},\ \bar{y}=\frac{y}{d},\ \bar{U}=\frac{U}{U_S},\ \bar{V}=\frac{V}{U_S},\ \bar{P}=\frac{P}{\rho_S U_S^2},\ \bar{T}=\frac{T-T_a}{T_S-T_a},\ \bar{C}=\frac{C}{C_S} \quad (2)$$

$$\bar{x}=\frac{x}{d},\ \bar{y}=\frac{y}{d},\ \bar{U}=\frac{U}{U_a},\ \bar{V}=\frac{V}{U_a},\ \bar{P}=\frac{P}{\rho_a U_a^2},\ \bar{T}=\frac{T-T_a}{T_S-T_a} \quad (3)$$

$U_s$, $T_s$ and $C_s$ are respectively the inlet velocity, inlet temperature and inlet concentration of the saline solution. The inlet velocity and the inlet temperature of the sweeping air are respectively $U_a$ and $T_a$.

Consequently, in non-dimension form, the governing equations and the boundary conditions in the hot domain are:

$$\frac{\partial \bar{U}}{\partial \bar{x}}+\frac{\partial \bar{V}}{\partial \bar{y}}=0 \quad (4)$$

$$\overline{U}\frac{\partial\overline{U}}{\partial\overline{x}}+\overline{V}\frac{\partial\overline{U}}{\partial\overline{y}}=-\frac{\partial\overline{P}}{\partial\overline{x}}+\frac{1}{\mathrm{Re}_S}\left(\frac{\partial^2\overline{U}}{\partial\overline{x}^2}+\frac{\partial^2\overline{U}}{\partial\overline{y}^2}\right) \tag{5}$$

$$\overline{U}\frac{\partial\overline{V}}{\partial\overline{x}}+\overline{V}\frac{\partial\overline{V}}{\partial\overline{y}}=-\frac{\partial\overline{P}}{\partial\overline{x}}+\frac{1}{\mathrm{Re}_S}\left(\frac{\partial^2\overline{V}}{\partial\overline{x}^2}+\frac{\partial^2\overline{V}}{\partial\overline{y}^2}\right) \tag{6}$$

$$\overline{U}\frac{\partial\overline{T}}{\partial\overline{x}}+\overline{V}\frac{\partial\overline{T}}{\partial\overline{y}}=\frac{1}{\mathrm{Re}_S\,\mathrm{Pr}_S}\left(\frac{\partial^2\overline{T}}{\partial\overline{x}^2}+\frac{\partial^2\overline{T}}{\partial\overline{y}^2}\right) \tag{7}$$

$$\overline{U}\frac{\partial\overline{C}}{\partial\overline{x}}+\overline{V}\frac{\partial\overline{C}}{\partial\overline{y}}=\frac{1}{\mathrm{Re}_S\,Sc_S}\left(\frac{\partial^2\overline{C}}{\partial\overline{x}^2}+\frac{\partial^2\overline{C}}{\partial\overline{y}^2}\right) \tag{8}$$

where the Reynolds, Prandlt and Schmidt of the hot saline solution are:

$$\mathrm{Re}_S=\frac{\rho_S U_S d}{\mu_S},\mathrm{Pr}_S=\frac{\mu_S Cp_S}{k_S},Sc_S=\frac{\upsilon_S}{D_S} \tag{9}$$

The boundary conditions in dimensionless form are:
- Inlet of the saline solution ($x$=0)

$$\overline{U}=1\ ,\ \overline{V}=0\ ,\ \overline{T}=1\ ,\ \overline{C}=1 \tag{10}$$

- Symmetry conditions ($y$=0)

$$\frac{\partial\overline{U}}{\partial\overline{y}}=0\ ,\ \frac{\partial\overline{T}}{\partial\overline{y}}=0\ ,\ \frac{\partial\overline{C}}{\partial\overline{y}}=0\ ,\ \overline{V}=0 \tag{11}$$

- Outlet of the saline solution ($x$=L)

$$\frac{\partial\overline{U}}{\partial\overline{x}}=0\ ,\ \frac{\partial\overline{V}}{\partial\overline{x}}=0\ ,\ \frac{\partial\overline{T}}{\partial\overline{x}}=0\ ,\ \frac{\partial\overline{C}}{\partial\overline{x}}=0 \tag{12}$$

- Feed saline solution-membrane interface ($y=d$)

Slip boundary condition, happened in the feed saline solution-membrane interface, due to hydrophobic membrane characteristics, is expressed by Eq. (13) and could be written using the dimensionless variables as:

$$\overline{U}=\frac{b}{d}\frac{\partial\overline{U}}{\partial\overline{y}} \tag{13}$$

In Eq. (13), $b$=0 refers to the non-slip boundary condition.

The remaining boundary conditions for feed saline solution-membrane interface are:

$$\overline{V}=\frac{J_v}{U_S\rho_S}\ ,\ \frac{\partial\overline{T}}{\partial\overline{y}}=\frac{d\left(Q_c+Q_L\right)}{k_S\left(T_a-T_S\right)}\ ,\ \frac{\partial\overline{C}}{\partial\overline{y}}=\frac{J_v d}{\rho_S D_S C_S} \tag{14}$$

where $Q_L=J_v h_{fg}$ represents the latent heat flux and $Q_c$ the conduction heat flux.

We assume that the generated vapor mass flow through the membrane is too small compared to the mass flow of sweeping air, so it does not modify the thermo-physical properties of the sweeping gas. Besides, we suppose that there is no solute (*NaCl*) in the permeate side.

The sweeping gas side equations and their boundary conditions are:

$$\frac{\partial\overline{U}}{\partial\overline{x}}+\frac{\partial\overline{V}}{\partial\overline{y}}=0 \tag{15}$$

$$\overline{U}\frac{\partial\overline{U}}{\partial\overline{x}}+\overline{V}\frac{\partial\overline{U}}{\partial\overline{y}}=-\frac{\partial\overline{P}}{\partial\overline{x}}+\frac{1}{\mathrm{Re}_a}\left(\frac{\partial^2\overline{U}}{\partial\overline{x}^2}+\frac{\partial^2\overline{U}}{\partial\overline{y}^2}\right) \tag{16}$$

$$\overline{U}\frac{\partial\overline{V}}{\partial\overline{x}}+\overline{V}\frac{\partial\overline{V}}{\partial\overline{y}}=-\frac{\partial\overline{P}}{\partial\overline{x}}+\frac{1}{\mathrm{Re}_a}\left(\frac{\partial^2\overline{V}}{\partial\overline{x}^2}+\frac{\partial^2\overline{V}}{\partial\overline{y}^2}\right) \tag{17}$$

$$\overline{U}\frac{\partial\overline{T}}{\partial\overline{x}}+\overline{V}\frac{\partial\overline{T}}{\partial\overline{y}}=\frac{1}{\mathrm{Re}_a\,\mathrm{Pr}_a}\left(\frac{\partial^2\overline{T}}{\partial\overline{x}^2}+\frac{\partial^2\overline{T}}{\partial\overline{y}^2}\right) \tag{18}$$

where the Reynolds and Prandlt numbers of the sweeping gas are:

$$\mathrm{Re}_a=\frac{\rho_a U_a d}{\mu_a},\mathrm{Pr}_a=\frac{\mu_a Cp_a}{k_a} \tag{19}$$

The boundary conditions in dimensionless form are:
- Inlet of the sweeping air domain ($x$=L)

$$\overline{U}=1\ ,\ \overline{V}=0\ ,\ \overline{T}=0 \tag{20}$$

- Symmetry conditions

$$\frac{\partial\overline{U}}{\partial\overline{y}}=0\ ,\ \frac{\partial\overline{T}}{\partial\overline{y}}=0\ ,\ \overline{V}=0 \tag{21}$$

- Outlet of the cold solution ($x$=0)

$$\frac{\partial\overline{U}}{\partial\overline{x}}=0\ ,\ \frac{\partial\overline{V}}{\partial\overline{x}}=0\ ,\ \frac{\partial\overline{T}}{\partial\overline{x}}=0 \tag{22}$$

- Sweeping gas-membrane interface ($y=d+\delta$)

$$\overline{U}=0 \tag{23}$$

$$\overline{V}=0 \tag{24}$$

$$\frac{\partial\overline{T}}{\partial\overline{y}}=\frac{d\left(Q_c+Q_L\right)}{k_S\left(T_a-T_S\right)} \tag{25}$$

Stephan's law is used to give the general mass flux form (Alklaibi and Lior 2005):

$$J_v=K\Delta P_v \tag{26}$$

where $J_v$ is the local vapor flux generated by the membrane, $K$ the permeability of the membrane and $\Delta P_v$ the water vapor pressure difference between the membrane sides;

The vapor pressure $P_v$ can be calculated using the Antoine's equation:

$$P_v = \exp\left(23.1964 - \frac{3816.44}{T - 46.13}\right) \quad (27)$$

The membrane permeability $K$ is defined as (Lawson and Lloyd 1997, Alklaibi and Lior 2006):

$$K = \frac{\varepsilon D_{v/a} M_v P_T}{\chi \delta_m P_{a,moy} R T_{moy,m}} \quad (28)$$

where $\varepsilon$ is the porosity of the membrane, $\chi$ is the tortuosity of the pores, $\delta$ is the membrane thickness [m], $D_{v/a}$ is the coefficient of vapor-air mass diffusion [m$^2$/s], $M_v$ is the Molar mass of water vapor [kg.kmol$^{-1}$], $P_T$ is the total pressure [Pa], $R$ is universal gas constant [J/kmol K], $P_{a,moy}$ is the average partial pressure of the air [Pa] and $T_{moy,m}$ is the average temperature of the membrane [°C].

The total pressure may be written as function of the water vapor pressure corresponding to the air side of the membrane and the humidity ratio $w$ (Khayet *et al.* 2000, Khayet *et al.* 2002):

$$P_T = \frac{P_v (w + 0.622)}{w} \quad (29)$$

The effect of salt's presence in the solution on the vapor pressure at the hot surface of the membrane side has been considered and the Raoult's Law is used. So that, the vapor pressure at the hot saline solution-membrane interface $P_{hm}$ is expressed as:

$$P_{hm} = P_v (1 - C_M) \quad (30)$$

where $C_M$ is the mole fraction of *NaCl* and $P_v$ is the vapor pressure calculated used Antoine's equation at the temperature of the hot saline-membrane interface.

The humidity ratio along the membrane module length may be related with the air flux, $m_a$, and with the humidity at the membrane module inlet $w_a$ (Khayet *et al.* 2000, Khayet *et al.* 2002):

$$w = w_a + \frac{J_v A}{m_a} \quad (31)$$

In the present study, the inlet air is considered as completely dry; therefore, $w_a$ will be considered equal to zero.

The total heat involved in such a process can be divided in two parts: the latent heat and the sensible one. The latent heat is associated with the evaporation of the liquid water at the hot membrane side. While, the sensible heat $Q_{sens}$ is transferred from the hot surface of the membrane.

To the sweeping air by heat conduction across the membranes $Q_c$ and the mass transfer of the vapor $Q_v$:

$$Q_{sens} = Qc + Qv = \frac{T_1 - T_2}{R_m} \quad (32)$$

where $T_1$ is the temperature at the hot side of the membrane, $T_2$ is the temperature at the cold side of the membrane and $R_m$ is the thermal resistance of the membrane defined by:

$$R_m = \frac{R_{mc} R_v}{R_{mc} + R_v} \quad (33)$$

where the heat transfer resistance of the solid part of the membrane is:

$$R_{mc} = \frac{\delta}{k_m} = \frac{\delta}{\varepsilon k_a + (1 - \varepsilon) k_{ma}} \quad (34)$$

$k_a$ and $k_{ma}$ are the thermal conductivity of the air, and the membrane material, respectively. The heat transfer resistance of the vapor flow through the membrane pores is:

$$R_v = \frac{1}{J_v C p_v} \quad (35)$$

The averaged permeate flux is defined as:

$$J = \frac{1}{L} \int_0^L J_v(x) dx \quad (36)$$

The averaged conduction heat flux is :

$$\overline{Q_C} = \frac{1}{L} \int_0^L Q_C(x) dx \quad (37)$$

The averaged total latent heat flux is:

$$\overline{Q_L} = \frac{1}{L} \int_0^L Q_L(x) dx \quad (38)$$

The total heat transfer is:

$$\overline{Q_T} = \frac{1}{L} \int_0^L Q_T(x) dx \quad (39)$$

Therefore, the process thermal efficiency can be defined as:

$$\eta = \frac{\overline{Q_L}}{\overline{Q_T}} \quad (40)$$

The local heat transfer coefficients, $h_{xs}$ and $h_{xa}$ respectively for the saline solution and the sweeping air are defined by making equal convective and conductive heat transfer at the hot saline-membrane interface and the membrane-air flow interface, respectively:

$$h_{xs} = \frac{-k_s}{T_0 - T_1} \frac{\partial T}{\partial y}\bigg|_{y=d} \quad (41)$$

$$h_{xa} = \frac{-k_a}{T_2 - T_3} \frac{\partial T}{\partial y}\bigg|_{y=d+\delta} \quad (42)$$

where $T_0$ represents the temperature at the center of the hot channel, $T_1$ the temperature at the saline solution-membrane interface, $T_2$ the temperature at the membrane-sweeping gas interface and $T_3$ the temperature at the center of cold channel.

Table 1 Influence of grid size on the permeate flux and the thermal efficiency

| *Nx,Ny* | | **1000,40** | **1200,40** | **1000,50** | **1200,50** |
|---|---|---|---|---|---|
| *J [kg/m²h]* | *b=0 µm* | 14.8287 | 14.8312 | 14.8425 | 14.8491 |
| | *b=50µm* | 15.1508 | 15.1539 | 15.1679 | 15.1752 |
| *η* | *b=0 µm* | 0.91469 | 0.91469 | 0.91470 | 0.91472 |
| | *b=50µm* | 0.91546 | 0.91547 | 0.91549 | 0.91550 |

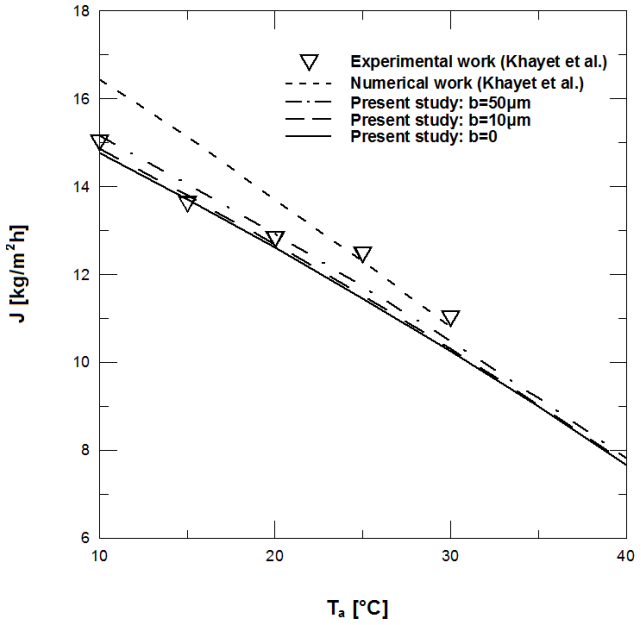


Fig. 2 Validation of the developed code with experimental data presented by Khayet *et al.* (2000)

## 3. Numerical method and validation

The governing equations with the boundary conditions are solved numerically using the finite volume method and the Simpler Algorithm (Versteeg and Malalasekera 2007). A grid-dependence analysis of the method of solution was performed as mentioned in Table 1. Based on a grid dependence analysis, the values are practically independent of the chosen grid, so we select the grid size of 1000,40 for the simulations conducted in the present study.

The validation of the developed numerical model is based on experimental results presented by Khayet *et al.* (2000), particularly the evolution of the permeate flux as a function of air inlet temperature. The experimental parameters used for the validation are:

- Membrane TF-450, characterized by a pore diameter equal to 0.45 mm, the thickness is equal to 178 mm and the fractional void volume is equal to 80%.

- Flow velocity equal to 0.15 m/s, air velocity equal to 0.8m/s and flow inlet temperature equal to 65°C.

The computed results for SGMD were validated by comparison with theoretical and experimental data of Khayet *et al.* (2000) and were found to be in very good agreement, as shown in Fig. 2. It is obvious that our model fits better the experimental data particularly when the slip condition is taken into consideration.

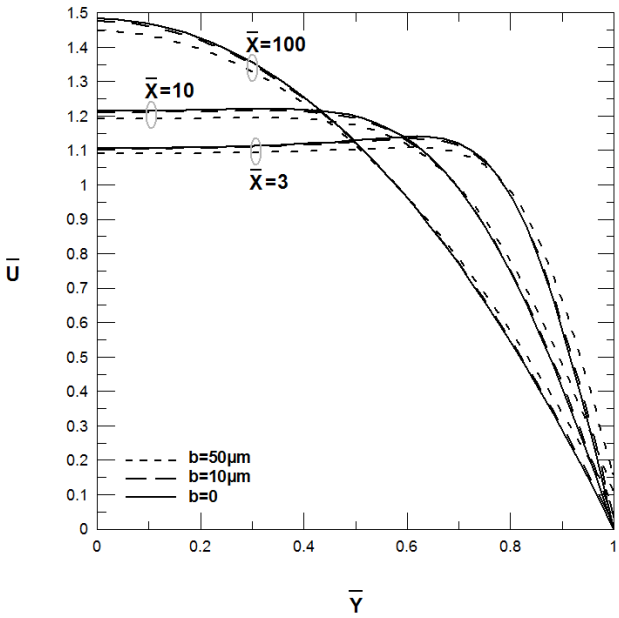


Fig. 3 Axial velocity evolutions at three positions for different slip lengths

Table 2 Slip length effects on process parameters

| *b [µm]* | 0 | 0.1 | 1 | 10 | 50 | 100 |
|---|---|---|---|---|---|---|
| *J[kg/m²h]* | 14.8287 | 14.8294 | 14.8357 | 14.8982 | 15.1508 | 15.4163 |
| *η* | 0.91469 | 0.91469 | 0.91470 | 0.91486 | 0.91546 | 0.91608 |

## 4. Results and discussion

The following general conditions were considered for all simulations: $d$=2mm, $L$=20cm, $U_a$=1m/s, $U_s$=0.1m/s, $C_s$=0.025, $T_a$=25°C, $\chi$=1.5, $\varepsilon$=0.8, $T_s$=70°C, $\delta$=0.4mm, $k_{ma}$=0.2W/mK.

In order to show the impact of introducing a slip velocity boundary condition on process parameters, we have presented pure water production $J$ and thermal efficiency $\eta$ for different slip lengths (Table 2). The slip length $b$ is varied from zero to 100 µm. For low values of $b$ (0-10µm), no significant effects on process parameters are noticed, while increasing b from 10 to 100 µm induces a notable variation of the permeate flux, $J$. The thermal efficiency remains almost unchanged.

The axial velocity profiles for different values of $x/d$ along the channel are presented in Fig. 3. It is important to notice that when the slip flow condition is applied ($b$ is nonzero), the fluid adjacent to the hydrophobic membrane no longer attains the velocity of the membrane's solid surface. In fact, increasing $b$ leads to an increase of the fluid velocity at the surface. In the core region of the channel, the saline solution accelerates and its maximum velocity occurs at the centerline of the channel, while slip condition tends to decelerate the centerline velocity.

This phenomenon is described clearly in fig. 4, where the evolutions of the centerline and wall saline solution velocities across the channel, for different values of $b$, are presented. It's clear that increasing slip length $b$ induces a decrease of the centerline velocity, while the fluid velocity at the wall is no longer zero.

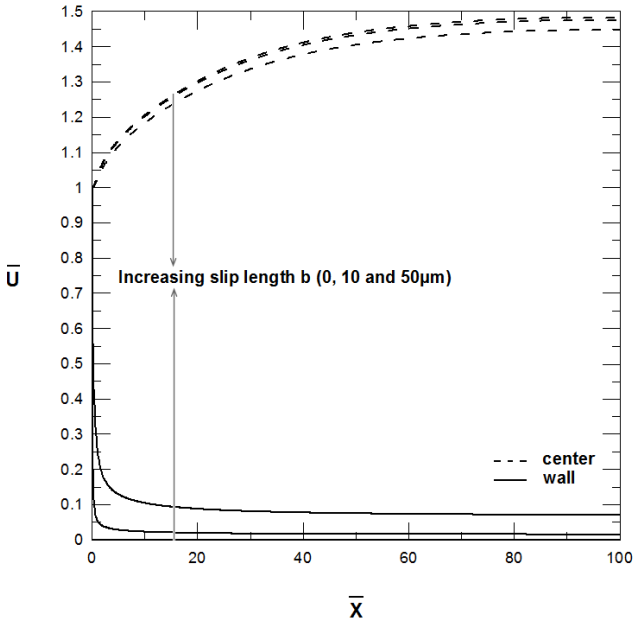


Fig. 4 Evolutions of the centerline and wall saline solution velocities as function of slip lengths

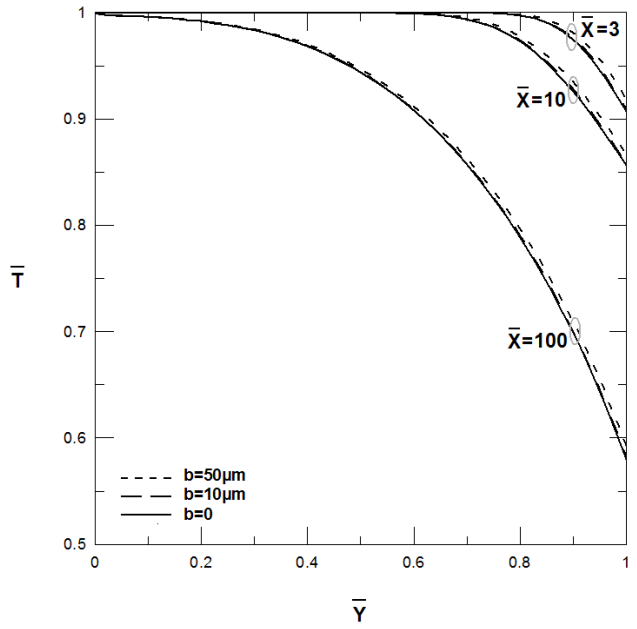


Fig. 5 Temperature evolutions at three axial positions for different slip lengths

The evolution of the temperature along the channel (positions *x/d*=3, 10 and 100) for different slip lengths is presented in Fig. 5. One can see that slip impact on the temperature profile is significant for high values of *b*. In fact, increasing *b* leads to a reduction of the temperature drop which results in a higher temperature difference and higher pure water production.

Fig. 6 presents the evolution of the permeate flux, the conductive heat flux and the thermal efficiency when varying the inlet temperature of the saline solution. Increasing $T_s$ induces an increase of all these parameters.

In fact, when neglecting slip condition, increasing $T_s$ from 40 to 80°C makes the permeate flux increase 7.35

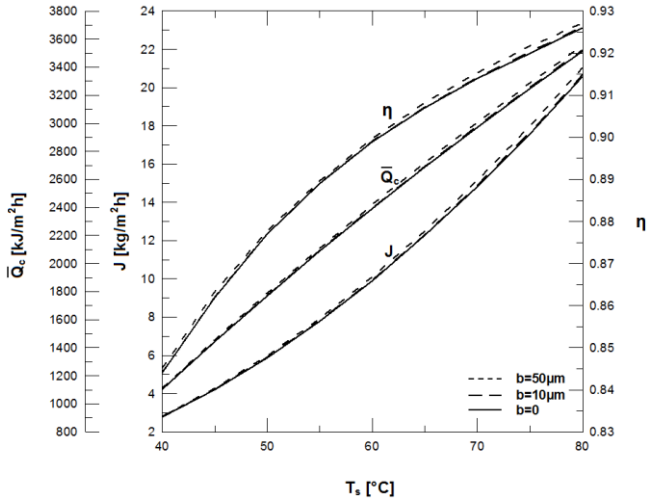


Fig. 6 Process parameters as function of inlet saline solution temperature and slip lengths

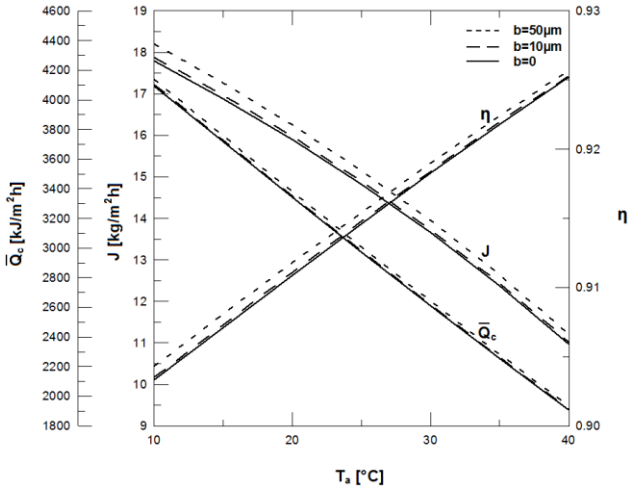


Fig. 7 Process parameters as function of inlet sweeping air temperature and slip lengths

times. The conductive heat flux and the thermal efficiency increase by 220% and 10% respectively. In the other side, introducing slip condition raises slightly pure water production, thermal efficiency and the conductive heat flux. This increase becomes significant for high values of slip length *b* and saline solution inlet temperature *Ts*. In fact for $T_s$ =80°C and *b* varying from zero to 50 µm, one can see an increase by 2% for both water production and conductive heat flux and 0.3% for thermal efficiency. No significant variation occurred when *b*=10 µm even for high values of *Ts*.

The effect of the temperature of the sweeping air on the SGMD configuration is mentioned in Fig. 7. When *b*=0, decreasing $T_a$ from 40 to 10°C leads to an increase of *J* by 62.4% and $Q_c$ by 114.7%, while $\eta$ decreases by 2%. The impact of slip velocity on process parameters is significant for all $T_a$ values. For $T_a$ =10°C, all quantities increase when b varies from zero to 50 µm. In fact *J*, $Q_c$ and $\eta$ increase by 3.4%, 1.3% and 0.15%, respectively.

Figs. 8-9 present the evolution of pure water production and thermal efficiency as a function of saline solution and

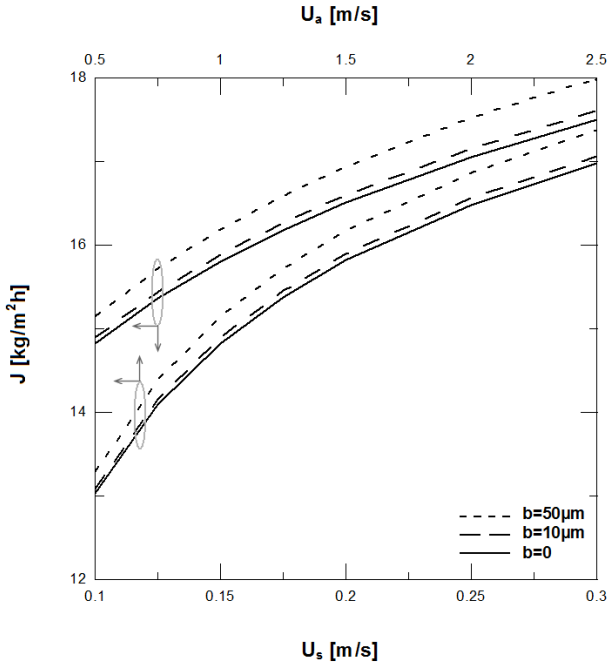


Fig. 8 Variation of pure water production for different inlet velocities and slip lengths

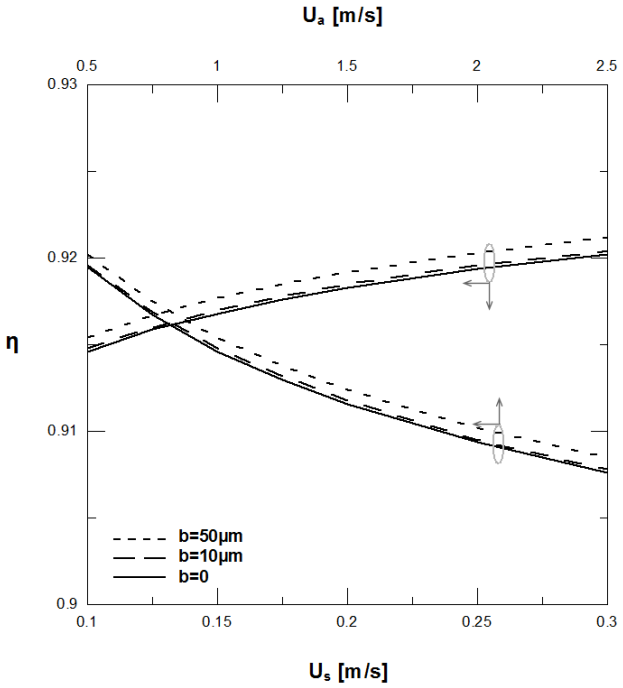


Fig. 9 Variation of thermal efficiency for different inlet velocities and slip lengths

sweeping air inlet velocities. For the non-slip condition, increasing inlet velocities results in an increasing water production by 26% and 18.3% respectively when $U_a$ increases from 0.5 to 2.5 m/s and $U_s$ from 0.1 to 0.3 m/s. The slip velocity impact is significant and could enhance by 3% the water production when $U_s$=0.3 m/s and the slip length varies from zero to 50 µm.

In the other side, increasing sweeping air velocity reduces thermal efficiency by 1.3% while increasing saline solution inlet velocity makes thermal efficiency rise by

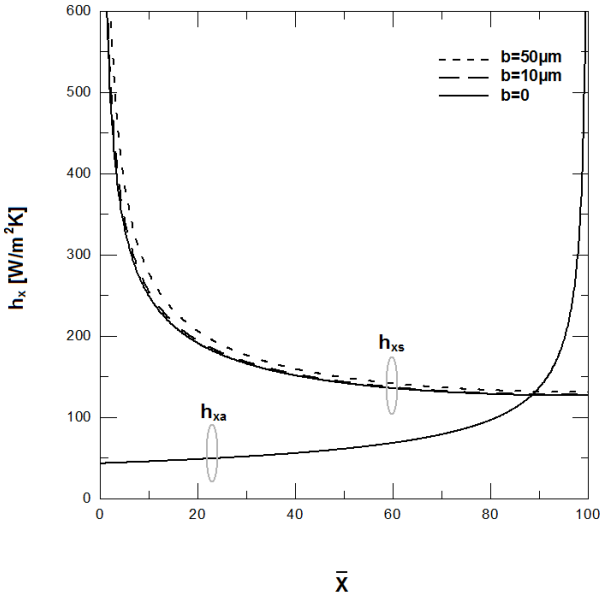


Fig. 10 Local heat transfer coefficients variations along the channel, $h_{xs}$ and $h_{xa}$ respectively for the saline solution and the sweeping air

0.8%, which presents opposite effects. The same behavior occurs when the slip boundary condition is considered, and varying $b$ from zero to 50 µm makes $\eta$ increase by 0.1% ($U_a$ =2.5 m/s).

Fig. 10 shows the variation of the convective heat transfer coefficients along the channel $h_{xs}$ and $h_{xa}$ for the saline solution and the sweeping air respectively. At the entrance of both saline solution and sweeping air, the temperature fields are under development. Therefore, heat transfer coefficients are high and decrease as the temperature fields approach the fully developed region. So, one can notice that the major heat transfer resistances of saline solution and sweeping air occurred at the feed side. On the other hand, when the slip condition is introduced, $h_{xs}$ increases while the behavior of $h_{xa}$ remains unchanged despite the variation of slip length from zero to 50µm. It is important to remind that the slip flow condition is applied on the feed water-membrane interface.

## 5. Conclusions

This study presents a numerical investigation of the heat and mass transfer in a sweeping gas membrane distillation unit used for desalination. The governing equations and their boundary conditions, including slip velocity due to the hydrophobic surface of the membrane, were developed and solved numerically using the finite volume method. The main results of this study are:

- All profiles and quantities are affected by the incorporation of the slip condition.
- The results of the complete theoretical model presented in this study, including slip velocity boundary condition, fit well with the experimental data.
- Slip effect on process parameters, particularly pure water production, becomes more pronounced at higher inlet

temperature of the saline solution, higher inlet velocities and lower sweeping gas temperature.

- Slip condition makes the local heat transfer of the saline solution rise across the channel while the behavior of the local heat transfer of the sweeping air remains unchanged despite the variation of slip length from zero to 50μm.

## Acknowledgement

The second author would like to thank the support of King Saud University, Deanship of Scientific Research, College of Engineering Research Center.

## References

Alklaibi, A.M. and Lior, N. (2005), "Transport analysis of air gap membrane distillation", *J. Membr. Sci.*, **255**(1-2), 239-253. https://doi.org/10.1016/j.memsci.2005.01.038.

Alklaibi, A.M. and Lior, N. (2006), "Heat and mass transfer resistance analysis of membrane distillation", *J. Membr. Sci.,* **282**(1-2), 362-369. https://doi.org/10.1016/j.memsci.2006.05.040

Camacho, L.M., Dumée, L., Zhang, J., Li, J., Duke, M., Gomez, J. and Gray, S. (2013), "Advances in Membrane Distillation for Water Desalination and Purification Applications", *Water,* **5**(1), 94-196. https://doi.org/10.3390/w5010094

Charfi, K., Khayet, M., and Safi, M.J. (2010), "Numerical simulation and experimental studies on heat and mass transfer using sweeping gas membrane distillation", *Desalination,* **259**(1-3), 84–96. https://doi.org/10.1016/j.desal.2010.04.028

Choi, C.H. and Kim, C.J. (2006), "Large slip of aqueous liquid flow over a nanoengineered superhydrophobic surface", *Phys. Rev. Lett.,*. **96**, 066001. https://doi.org/10.1103/PhysRevLett.96.066001

Cojocaru, C. and Khayet, M. (2011), "Sweeping gas membrane distillation of sucrose aqueous solutions: Response surface modeling and optimization", *Separation Purification Technol.,,* **81**(1), 12-24. https://doi.org/10.1016/j.seppur.2011.06.031

Cottin, B.C., Cross, B., Steinberger, A. and Charlaix, E. (2005), "Boundary slip on smooth hydrophobic surfaces: intrinsic effects and possible artifacts", *Phys. Rev. Lett.,* **94**(5), 056102. https://doi.org/ 10.1103/PhysRevLett.94.056102

Duyen, P.M., Paul, J., Romchat, R. and Chettiyapan, V. (2016), "Feasability of sweeping gas membrane distillation on concentrating triethylene glycol from waste streams", *Chem. Eng. Process. Process Intensification*, **110**, 225-234. https://doi.org/10.1016/j.cep.2016.10.015

El-Bourawi, M.S., Ding, Z., Ma, R. and Khayet, M. (2006), "Framework for better understanding membrane distillation separation process'', *J. Membr. Sci.*, **285**(1-2), 4-29. https://doi.org/10.1016/j.memsci.2006.08.002

Jun Liu, J., Li, X., Zhang, W., Li, B., and Liu, C. (2020), "Superhydrophobic-slip surface based heat and mass transfer mechanism in vacuum membrane distillation", *J. Membr. Sci.*, **614**, 118505. https://doi.org/10.1016/j.memsci.2020.118505

Khayet, M., Godino, M.P. and Mengual, J.I. (2003), "Theoretical and experimental studies on desalination using the sweeping gas membranedistillation method", *Desalination*, **157**(1-3), 297-305. https://doi.org/10.1016/S0011-9164(03)00409-0.

Khayet, M., Godino, P. and Mengual, J.I. (2000), "Nature of flow on sweeping gas membrane distillation", *J. Membr. Sci.*, 2000, **170**(2), 243-255. https://doi.org/10.1016/S0376-7388(99)00369-5.

Khayet, M., Godino, M.P. and Mengual, J.I. (2002), "Thermal boundary layers in sweeping gas membrane distillation processes", *AIChE J.*, **48**(7), 1488-1497. https://doi.org/10.1002/aic.690480713.

Lawson, K.W. and Lloyd, D.R. (1997), "Membrane distillation", *J. Membr. Sci.,* **124**(1), 1-25. https://doi.org/10.1016/S0376-7388(96)00236-0.

Lee, C.H. and Won, H.H. (2001), "Effect of operating variables on the flux and selectivity in sweep gas membrane distillation for dilute aqueous isopropanol", *J. Membr. Sci.,*, **188**(1), 79–86.https://doi.org/10.1016/S0376-7388(01)00373-8.

Lee, C., Choi, C.H. and Kim, C.J. (2008), "Structured surfaces for giant liquid slip". *Phys. Rev. Lett.,* **101**, 064501. https://doi.org/10.1103/PhysRevLett.101.064501.

Loussif, N. and Orfi, J. (2016), "Comparative study of air gap, direct contact and sweeping gas membrane distillation", *Membr. Water Treat.*, **7**(1), 71-86. https://doi.org/10.12989/mwt.2016.7.1.071.

Moore, S.E., Mirchandani, S.D., Karanikola, V., Nenoff, T.M., Arnold, R.G. and Saez, A.E. (2018), "Process modeling for economic optimization of a solar driven sweeping gas membrane distillation desalination system", *Desalination,* **437**, 108-120. https://doi.org/10.1016/j.desal.2018.03.005.

Orfi, J., Loussif, N., Davies, P.A. (2016), "Heat and mass transfer in membrane distillation used for desalination with slip flow", *Desalination*, **381**, 135-142. https://doi.org/10.1016/j.desal.2015.12.009.

Ou, J. and Rothstein, J.P. (2005), "Direct velocity measurements of the flow past drag-reducing ultrahydrophobic surfaces", *Phys. Fluids,* **17**, 103606. https://doi.org/10.1063/1.2109867

Pit, R., Hervet, H. and Leger, L. (2000), "Direct experimental evidence of slip in hexadecane:solid interfaces", *Phys. Rev. Lett.,,* **85**(5), 980. https://doi.org/10.1103/PhysRevLett.85.980

Ramon, G., Agnon, Y. and Dosoretz, C. (2009), "Heat transfer in vacuum membrane distillation: Effect of velocity slip", *J. Membr. Sci.,* **331**(1-2), 117-125. https://doi.org/10.1016/j.memsci.2009.01.022

Rivier, C.A., Garcia-Payo, M.C., Marison, I.W. and Stockar, U.V. (2002), "Separation of binary mixtures by thermostatic sweeping gas membrane distillation I. Theory and simulations", *J. Membr. Sci.,* **201**(1-2), 1–16. https://doi.org/10.1016/S0376-7388(01)00648-2.

Rommel, M., Koschikowski, J. and Wieghaus M. (2007), "Solar Driven Desalination systems based on Membrane desalination", *Solar Desalination for the 21st Century*, 247-257.

Shukla, S., Méricq, J.P., Belleville, M.P., Hengl, N., Benes, N.E., Vankelecom, I. and Marcano, J.S. (2018), "Process intensification by coupling the Joule effect with pervaporation and sweeping gas membrane distillation", *J. Membr. Sci.,* **545**, 150-157. https://doi.org/10.1016/j.memsci.2017.09.061.

Si, M.H., Chen, Y.H., Yuan, W.Z., Zhao, S., Hong, Y., Yed, W.B. and Yang, M. (2019), "Heat and mass transfer in a hollow fiber membrane contactor for sweeping gas membrane distillation", *Separation Purification Technol.,* **220**, 334–344. https://doi.org/10.1016/j.seppur.2019.03.046.

Tretheway, D.C. and Meinhart, C.D. (2004), "A generating mechanism for apparent fluid slip in hydrophobic microchannels", *Phys. Fluids*, **16**, 1509. https://doi.org/10.1063/1.1669400.

Tretheway, D.C. and Meinhart, C.D. (2002), "Apparent fluid slip at hydrophobic microchannel walls", *Phys. Fluids,* **14**, L9. https://doi.org/10.1063/1.1432696.

Versteeg, K. and Malalasekera, W. (2007), *An Introduction to Computational Fluid Dynamics: The Finite Volume Method*, (2nd edition), Pearson and Prentice Hall, London.

Xie, Z., Duong, T., Hoang, M., Nguyen, C. and Bolto, B. (2009), "Ammonia removal by sweep gas membrane distillation", *Water Res.*, **43**(6), 1693-1699. https://doi.org/10.1016/j.watres.2008.12.052.

*CC*

## Appendix

### *Nomenclature*

| | |
|---|---|
| $A$ | Membrane area [$m^2$] |
| $C$ | Mass fraction of NaCl |
| $C_M$ | Mole fraction of NaCl |
| $C_p$ | Specific heat [$Jkg^{-1}K^{-1}$] |
| $d$ | half-width of the flow channel [m] |
| $D_s$ | Diffusion coefficient of NaCl [$m^2/s$] |
| $D_{v/a}$ | Coefficient of vapor-air mass diffusion [$m^2/s$] |
| $g$ | Acceleration of gravity [$m/s^2$] |
| $h_{fg}$ | Latent heat of evaporation [J/kg] |
| $h_x$ | Local convective heat transfer coefficient [$W/m^2K$] |
| $J$ | length-averaged permeate flux [$kg/m^2h$] |
| $J_v$ | local permeate flux at the hot side of membrane [$kg/m^2s$] |
| $K$ | permeability of the membrane |
| $k$ | Thermal conductivity [W/mK] |
| $L$ | Membrane length [m] |
| $m_a$ | Air flux [kg/s] |
| $M_v$ | Molar mass of water vapor [$kg.kmol^{-1}$] |
| $N_x$ | Number of nodes along x direction |
| $N_y$ | Number of nodes along y direction |
| $P$ | pressure [Pa] |
| $Pr$ | Prandtl number |
| $Q_C$ | Conductive heat flux [$kJ/m^2h$] |
| $Q_L$ | Latent heat flux [$kJ/m^2h$] |
| $Q_T$ | Total flux [$kJ/m^2h$] |
| $R$ | Universal gas constant [J/kmol K] |
| $Re$ | Reynolds number |
| $R_m$ | Thermal resistance of the membrane [$m^2K/W$] |
| $R_{mc}$ | Thermal resistance of the solid part of the membrane [$m^2K/W$] |
| $R_v$ | Thermal resistance of the vapor through pores [$m^2K/W$] |
| $Sc$ | Schmidt number |
| $T$ | temperature [°C] |
| $U$ | axial velocity component [m/s] |
| $V$ | radial velocity component [m/s] |
| $w$ | Humidity ratio |
| $w_a$ | humidity at the membrane module inlet |
| $x$ | Coordinate along to the solution flow [m] |
| $y$ | coordinate normal to the solution flow [m] |

*Greek letters*

| | |
|---|---|
| $\mu$ | Dynamic viscosity [$kg.m^{-1}s^{-1}$] |
| $\upsilon$ | Cinematic viscosity [$m^2s^{-1}$] |
| $\rho$ | Density [$kg.m^{-3}$] |
| $\varepsilon$ | Porosity |
| $\chi$ | Tortuosity |
| $\delta$ | Membrane thickness [m] |
| $\eta$ | Process thermal efficiency |

*Subscripts*

| | |
|---|---|
| $a$ | air |
| $m$ | membrane |
| $ma$ | membrane material |
| $moy$ | Average |
| $s$ | saline solution |
| $T$ | total |
| $v$ | vapor |